JACS
JOURNAL OF THE AMERICAN CHEMICAL SOCIETY

Article

pubs.acs.org/JACS

Construction of LRET-Based Nanoprobe Using Upconversion Nanoparticles with Confined Emitters and Bared Surface as Luminophore

Zhen Li, Songwei Lv, Yali Wang, Shiyu Chen, and Zhihong Liu*

Key Laboratory of Analytical Chemistry for Biology and Medicine (Ministry of Education), College of Chemistry and Molecular Sciences, Wuhan University, Wuhan 430072, China

Supporting Information

ABSTRACT: Upconversion nanoparticles (UCNPs) are promising energy donors for luminescence resonance energy transfer (LRET) and have widely been used to construct nanoprobes. To improve the LRET efficiency, which is currently a limiting factor for UCNPs-based bioassay, we herein propose a strategy to construct LRET-based nanoprobe using UCNPs with confined emitters and bared surface as the luminophore, with Ca^{2+} as the proof-of-concept target. The sandwich-structure upconversion nanoparticles (SWUCNPs) are designed with a core-inner shell-outer shell architecture, in which the emitting ions (Ln^{3+}) are precisely located in the inner shell near the particle surface, which is close enough to external energy acceptors. The target receptor (Fluo-4) is directly tagged on bared surface of SWUCNPs, which further reduces the donor-to-acceptor distance. Our strategy contributes to significantly improved LRET efficiency and hence affords an ultrahigh sensitivity for Ca^{2+} detection. The as-constructed nanoprobe is structurally stable and exhibits good biocompatibility, which ensures uptake and reliable observation in living cells. The nanoprobe can be used for monitoring the different levels of cytosol [Ca^{2+}] in living cells. Furthermore, it is applicable in Ca^{2+} imaging in mice liver tissues.

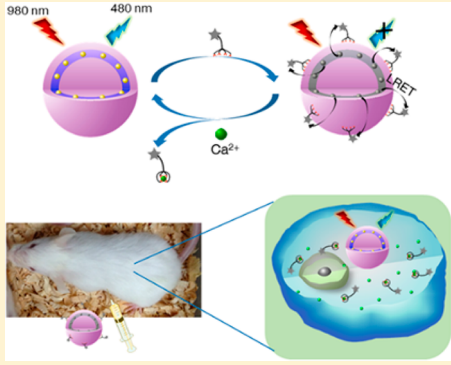

INTRODUCTION

Upconversion nanoparticles (UCNPs) have widely been used to construct nanoprobes in the past several years, because of their near-infrared (NIR)-excitation nature which minimizes autofluorescence from biomolecules and interference from scattered light.[1−12] In most cases, such nanoprobes are based on luminescence resonance energy transfer (LRET) with UCNPs as energy donors. This is particularly owing to the anti-Stokes emission of UCNPs which eliminates co-excitation of the donor−acceptor pair and thus precludes possible false positive signals from the acceptor.[13−19] Despite the great success and the ongoing increase of interest with UCNPs-based bioassay, there is an intractable problem with UCNPs as energy donor, i.e., the limited energy-transfer efficiency from UCNPs to small-molecule energy acceptors which in general also act as the recognizing domain of targets. The limitation in LRET efficiency may somehow lower signal-to-background ratios and hence impairs the assay sensitivities.[20−23]

The deficiency is originated mainly from two facts. The first one is the structural character of upconversion nanomaterials. As known, LRET efficiency is highly dependent on the donor-to-acceptor distance, and the nonradiative energy transfer is effective generally within a distance of 10 nm. Since the scale of currently used UCNPs is normally at tens of nanometers, only those emitting ions (doped rare earth ions) near the surface of the nanoparticles are in the effective energy-transfer range and quenchable.[24−26] Quite a large part of emitters are out of the energy-transfer distance and nonquenchable, leading to considerable background. The second factor hindering energy transfer is the employment of various surface ligands on UCNPs, which are designed mainly to assist the conjugation with receptors. However, the existence of these ligands inevitably increases the distance from the emitters to the quenchers.

Some efforts have been made to address this issue. Sub-10 nm homogeneous UCNPs can shorten the donor−acceptor distance owing to their smaller diameter.[27,28] But these materials are susceptible to severe environmental quenching.[29] On the other hand, several kinds of inorganic nanosized quenchers are able to provide higher energy-transfer efficiencies possibly due to the surface energy-transfer mechanism,[30−32] but the introduction of nanosized quenchers may decrease thermodynamic stability and compromise biocompatibility. In the meanwhile, nanosized quenchers are not as flexible as small-molecule receptors to be integrated in the probe as a recognizing domain.

To deal with the problems, we herein propose the strategy to use UCNPs with confined emitters and bared surface as the luminophore (energy donor), with which a LRET-based nanoprobe for intracellular Ca^{2+} is constructed. In view of the distance dependence of LRET, one can reasonably expect an

Received: February 10, 2015
Published: February 24, 2015

DOI: 10.1021/jacs.5b01504
J. Am. Chem. Soc. 2015, 137, 3421−3427

increased energy-transfer efficiency if more emitters are located near the surface of UCNPs. But it is too challenging to achieve such controlled distribution of ions in traditional homogeneous UCNPs, because it is difficult to specifically localize the doped ions (emitters) in the host matrix ($NaYF_4$ crystal, for example). Hence we fabricate a sandwich structure with a layer-by-layer seed-mediated shell growth strategy,[33−35] which enables precise localization of the emitters in the host matrix, i.e., most emitting ions are confined in a thin layer near the surface so that they can be very close to external quenchers. In another aspect, we avoid using any surface ligand to connect a specific receptor (Fluo-4 for calcium in this work, also acting as the energy acceptor). Instead, we directly make use of the rare earth ions on the uncovered UCNPs to coordinate with the receptor, through which the donor-to-acceptor distance can be minimized. Our strategy provides a new type of upconversion nanoprobe with significantly improved LRET efficiency and ultrahigh sensitivity, suitable for cell and tissue imaging.

EXPERIMENTAL SECTION

Synthesis of Oleic Acid Stabilized SWUCNPs. Oleic acid (OA) stabilized $NaYF_4$@$NaYF_4$:Ln^{3+}@$NaYF_4$ SWUCNPs were synthesized according to the seed-mediated method developed previously.[34] Yb^{3+}, Er^{3+}, or Tm^{3+} were used as the doping ions (Ln^{3+}), depending on emission wavelength in demand. In a typical procedure, 1 mmol of $Y(oleate)_3$, 20 mmol of NaF, and 20 mL of OA/1-octadecene (ODE) (v/v = 1:1) mixed solvent were added to a 100 mL three-necked flask simultaneously and degassed at 110 °C for 1 h under vacuum to remove residual water and oxygen. Then the mixture was heated to 320 °C and kept for 75 min in argon atmosphere. After that, 4 mL of the reaction mixture was retrieved followed by injection of 0.4 mmol $Ln(oleate)_3$ dissolved in OA/ODE (8 mL, v/v = 1:1) and kept at 320 °C for 20 min. Six mL of the reaction mixture was retrieved followed by injection of 0.4 mmol $Y(oleate)_3$ dissolved in OA/ODE (8 mL, v/v = 1:1) and kept at 320 °C for 20 min. Then each aliquot was precipitated by adding equal volumes of ethanol at room temperature. Finally the resultant mixtures were centrifugally separated and washed six times with hexane/ethanol (v/v = 1:1) mixture solvent. The products $NaYF_4$, $NaYF_4$@$NaYF_4$:Ln^{3+} and $NaYF_4$@$NaYF_4$:Ln^{3+}@$NaYF_4$ were thus obtained. By using different amounts of the shell precursors and a fixed amount of the seeds, SWUCNPs with different thicknesses of shells were obtained.

$NaYF_4$:Ln^{3+} homogeneous UCNPs were prepared in the same way with the $NaYF_4$ core.

Synthesis of PAA Stabilized UCNPs. PAA stabilized UCNPs were prepared through a ligand exchange procedure at the liquid−liquid interface.[10,36] 30 mg of the OA capped UCNPs in chloroform (4 mL) were slowly added into a water solution (8 mL) containing 200 mg PAA, and the solution was vigorously stirred for 24 h. Afterward, the nanoparticles were transferred into the upper water layer from the chloroform layer due to the PAA attachment. The nanoparticles were separated by centrifugation and washed with ultrapure water to gain PAA stabilized UCNPs.

Preparation of Bared SWUCNPs. Bared SWUCNPs, i.e., $NaYF_4$@$NaYF_4$:Yb,Tm@$NaYF_4$ were prepared by removing the surface ligands through acid treatment.[37,38] 60 mg of the oleate-capped SWUCNPs were dispersed in 30 mL of acidic ethanol solution (pH = 1) and ultrasonicated for 1 h to remove the oleate ligands. After the reaction was completed the SWUCNPs were collected by centrifugation and further purified by adding an acidic ethanol solution (pH = 4). The resulting bared SWUCNPs were washed with ethanol and ultrapure water several times and redispersed in ultrapure water.

Preparation of the SWUCNPs-Fluo-4 Nanoprobe. The bared $NaYF_4$@$NaYF_4$:Yb,Tm@$NaYF_4$ SWUCNPs (3 mg) were dispersed in MOPS buffer (10 mM, pH 7.2, 100 mM KCl), and 40 nmol of aqueous solution of Fluo-4 was added. The mixture solution was shaken gently overnight and then centrifuged to remove the excess Fluo-4. The resulting products were washed with ultrapure water several times and then redispersed in MOPS buffer to a final concentration of 1 mg/mL for further use.

***In Vitro* Assay of Ca^{2+} with SWUCNPs-Fluo-4 Nanoprobe.** In MOPS buffer (10 mM, pH 7.2, 100 mM KCl, 10 mM EGTA), 0.075 mg/mL SWUCNPs-Fluo-4 conjugate was incubated with various concentrations of Ca^{2+} for 3 h. The final concentrations of total Ca^{2+} were 0, 0.001, 0.005, 0.01, 0.1, 0.5, 1, 2, 3, 4, 5, 7, 9 mM, respectively. And the free [Ca^{2+}] was controlled by EGTA to be 0, 0.015, 0.075, 0.151, 1.52, 7.95, 16.7, 37.7, 64.7, 100, 151, 352, and 1350 nM, respectively.[39,40] The mixtures were then subject to luminescence measurement excited with 980 nm continuous-wave laser.

Cell Culture. The cell lines HeLa were seeded in a 24-well plate with cover glasses and cultured in Dulbecco's modified Eagle's medium (DMEM) supplemented with 10% fetal bovine serum (FBS), 100 U/mL penicillin, and 100 μg/mL streptomycin at 37 °C and 5% CO_2 for 24 h.

Cytotoxicity Evaluation. The *in vitro* cytotoxicity was measured by MTT assay. HeLa cells were cultivated in 96-well plates containing DMEM at 37 °C and 5% CO_2 for 12 h. Subsequently, the medium was substituted for fresh medium supplemented with varying concentrations UCNPs-Fluo-4 conjugate (0, 0.1, 0.2, 0.3, 0.4, 0.5, 0.6 mg/mL). Each concentration of nanoparticles was performed repeatedly 3 times. After 24 h, cells were washed with PBS twice and incubated with 0.5 mg/mL MTT reagent at 37 °C for 4 h. After the addition of dimethyl sulfoxide (DMSO) to dissolve the formazan crystals, the absorbance of each well at 490 nm was measured by a microplate reader. The following formula was applied to calculate the cell survival rate: Cell viability (%) = (mean Abs. of treatment group/mean Abs. of control) × 100%.

Detection of Cytosol [Ca^{2+}] in Living Cells. HeLa cells were rinsed with phosphate buffered saline (PBS) (pH 7.2, 137 mM NaCl, 2.7 mM KCl, 10 mM Na_2HPO_4, 1.8 mM KH_2PO_4) three times, and then adherent cells were incubated with 0.3 mg/mL SWUCNPs-Fluo-4 conjugate in PBS for 1.5 h at 37 °C under 5% CO_2 and then washed with PBS sufficiently to remove excess nanoparticles. For negative and positive groups, the cells were treated with EGTA and ATP, respectively, for 10 min at 37 °C both before and after labeling. To test the effects of the inhibition of calcium influx into endoplasmic reticulum (ER), a group of cells were pre-incubated with the inhibitor thapsigargin (5 μM) for 10 min at 37 °C in the incubator.

Ca^{2+} Imaging in Mice Liver Tissues. Kunming mice (~30 g) were intraperitoneally (i.p.) injected with different concentrations of $CaCl_2$ (0, 4.0, and 8.0 mg/100 g body weight in 200 μL of physiological saline, respectively). After 30 min, the mice were subsequently injected with SWUCNPs-Fluo-4 conjugate (3 mg/100 g body weight in 300 μL physiological saline). For the negative control group, the mice were pretreated with EGTA (10 mg/100 g body weight in 200 μL of physiological saline) for 30 min before injecting the nanoprobe. To test the inhibition of influx of extracellular calcium, a group of mice were pretreated with verapamil (1.0 mg/100 g body weight in 200 μL of physiological saline), a Ca^{2+} channel blocker for 30 min before injection of $CaCl_2$. Livers were harvested 1 h after the injection of the nanoprobe and sliced for upconversion luminescence imaging.

RESULTS AND DISCUSSION

Principle of the LRET-Based Ca^{2+} Nanoprobe. As depicted in Scheme 1, the upconversion energy donor is designed with a sandwich structure comprising the core, inner shell, and outer shell. The core of the material is the host matrix ($NaYF_4$ nanoparticle) without doped ions, while the emitters (doped Ln^{3+} ions) are confined in the inner shell layer. To protect the emitters from environmental quenching, another $NaYF_4$ shell is further deposited on the surface of the inner shell to form the sandwich structure. Both the inner and outer shells are controlled with a thickness of a few nanometers. With

DOI: 10.1021/jacs.5b01504
J. Am. Chem. Soc. 2015, 137, 3421−3427

Scheme 1. Schematic Illustration (not to real scale) of the NIR Nanoprobe for Calcium Based on LRET from SWUCNPs with Bared Surface to Fluo-4

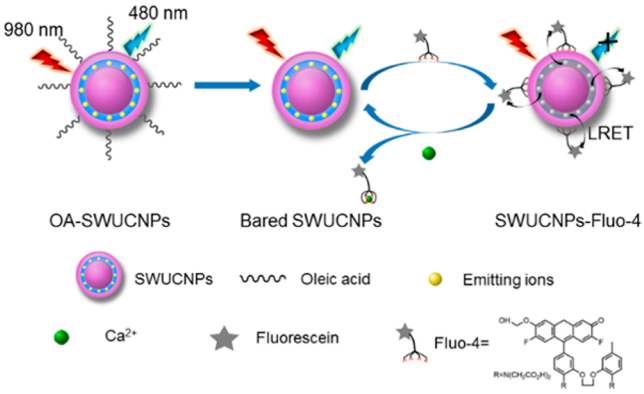

such structural innovation of UCNPs, most emitting ions are positioned near the surface of the material and close to external energy acceptors, which is in favor of the LRET process. Further, the surface ligands of SWUCNPs are removed via acid treatment to acquire bared SWUCNPs. The specific receptor for Ca^{2+}, Fluo-4 derived from fluorescein with BAPTA, is used as both the target recognizing motif and the energy acceptor, with the fluorescein molecule as the luminescence quencher. Fluo-4 is directly linked to bared SWUCNPs via the coordination between carboxyl on BAPTA and the exposed Ln^{3+} ions on SWUCNPs. The SWUCNPs-Fluo4 nanoprobe is weakly luminescent due to the efficient energy transfer from emitting Ln^{3+} ions to fluorescein. The introduction of Ca^{2+} leads to recovery of the luminescence of SWUCNPs, because the strong affinity of BAPTA toward Ca^{2+} causes the detachment of Fluo-4 from the surface of SWUCNPs, which thus inhibits the LRET process.

Properties of the Sandwich-Structured UCNPs. The sandwich-structure $NaYF_4$@$NaYF_4$:Yb,Er@$NaYF_4$ particles were synthesized using a layer-by-layer seed-mediated shell growth strategy with OA as the capping agent (Figure 1a). Transmission electron microscopy (TEM) images of the as-synthesized nanoparticles (Figure 1b–d) clearly show the size evolution of the materials, i.e., from the $NaYF_4$ core with an average diameter of ~23.4 nm to the $NaYF_4$@$NaYF_4$:Yb,Er core-inner shell structure (~27.1 nm) and finally to the $NaYF_4$@$NaYF_4$:Yb,Er@$NaYF_4$ sandwich structure (~31.0 nm). According to the size histograms obtained from the large area TEM images, the size distributions of all these materials are quite narrow (σ < 5%), indicating the fine control of the material morphology by the growth pathway. The X-ray diffraction (XRD, Supporting Information (SI) Figure S1a) patterns indicate that the obtained nanoparticles are with a hexagonal phase, which is consistent with the analysis of selected area electron diffraction (SAED, SI Figure S1b). The high angle annular dark field image (HAADF) and two-dimensional (2D) elemental mapping by energy-dispersive X-ray spectroscopy (EDS) confirm that the Yb^{3+} and Er^{3+} ions distribute mainly in the inner shell of SWUCNPs (Figure 1e). To protect the emitting ions from environmental quenching, we deposited a protecting layer (the outer $NaYF_4$ shell) to prevent the quenching. As Figure 1f shows, the introduction of a layer of $NaYF_4$ (the outer shell) with ca. 2.0 nm thickness leads to a dramatic enhancement of luminescence intensity, as compared with the core-inner shell material. Although the

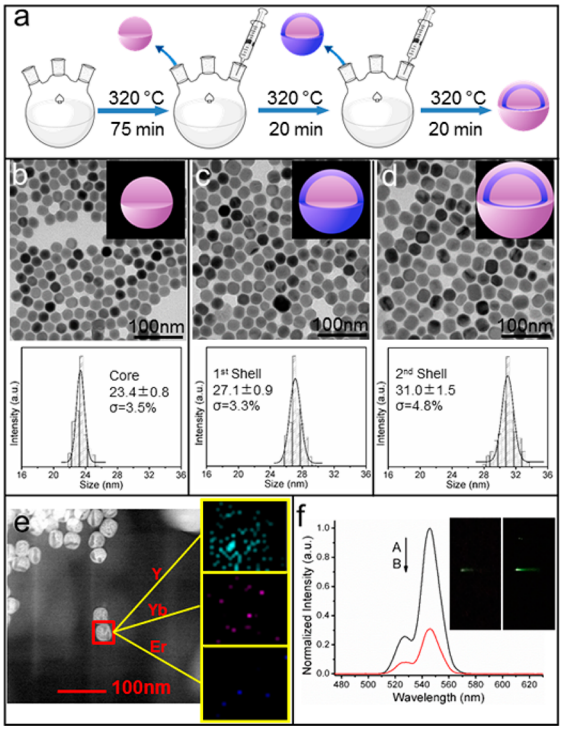

Figure 1. (a) Preparation of $NaYF_4$@$NaYF_4$:Yb,Er@$NaYF_4$ sandwich structure through a layer-by-layer seed-mediated shell growth method. (b–d) TEM images and size distribution of $NaYF_4$ core (b), core-inner shell structure $NaYF_4$@$NaYF_4$:Yb,Er (c), and $NaYF_4$@$NaYF_4$:Yb,Er@$NaYF_4$ sandwich structure (d). (e) HAADF image of the sandwich material. Inset: EDS 2D mapping of the distribution of Y^{3+}, Yb^{3+}, and Er^{3+} ions. (f) The upconversion emission spectra of the core-inner shell material (curve B) and the sandwich material (curve A) dispersed in chloroform; inset: corresponding photographs of the two solutions excited at 980 nm. Note: the concentration of the core-inner shell material was 10^4 times higher than that of the sandwich material.

concentration of the sandwich material is lower than that of the core–shell material by 4 orders of magnitude, its luminescence intensity is still >3 times higher than the latter.

Improved LRET Efficiency of SWUCNPs. The improvement of LRET efficiency from SWUCNPs was verified by comparing with homogeneous UCNPs. The hydrophobic SWUCNPs (with OA as ligands) were first transferred into water-dispersible materials by using poly(acrylic acid) (PAA) molecules to replace the original OA ligands through ligand exchange at the liquid–liquid interface[10,36] (SI Figure S2). The successful loading of PAA is confirmed by Fourier transform infrared (FTIR) analysis (SI Figure S3a). The XRD patterns and TEM images show that the ligand-exchange process has no obvious adverse effects on the crystalline phase and morphology of the materials (SI Figure S3b,c). Besides, ca. 40% of the photoluminescence intensity of SWUCNPs is maintained after PAA modification (SI Figure S3d). We then compared the energy-transfer efficiencies from SWUCNPs and that from traditional homogeneous UCNPs, i.e., $NaYF_4$:Yb,Er, to a common energy acceptor. To also illustrate the adjustability of energy-transfer efficiency of SWUCNPs, we synthesized two batches of SWUCNPs with different thicknesses of the shells in this experiment. By using different amounts of the shell precursors and a fixed amount of the seeds, the shell thicknesses of the two materials were acquired

DOI: 10.1021/jacs.5b01504
J. Am. Chem. Soc. 2015, 137, 3421–3427

as approximately 2.5 nm (SI Figure S4a–c, named as SWUCNP-2.5 for short) and 4.0 nm (SI Figure S4d–f, named as SWUCNP-4), respectively. The particle size of homogeneous UCNPs was controlled to be equal to that of SWUCNP-2.5 (SI Figure S4g). We selected an amine tagged organic dye lissamin rhodamine B ethylenediamine as the energy acceptor, which is positively charged in near-neutral conditions and can be adsorbed onto the surface of UCNPs via electrostatic attraction with the negatively charged PAA molecules. The dye has a broad absorption band covering 520–580 nm (SI Figure S5) that overlaps with the luminescence emission of UCNPs at 550 nm and thus ensures the nonradiative energy transfer. To prove the LRET mechanism, we performed time-resolved luminescence measurements. It is seen that the lifetime of the UCNPs is significantly reduced by the dye, and the degree of lifetime reduction is dependent on the amount of dye (SI Figure S6), which indicates the occurrence of nonradiative energy transfer. The energy-transfer efficiencies of the three energy donors were compared by measuring their luminescence quenching degrees at the same concentration ratios of dyes over UCNPs (the concentrations of different samples were normalized with particle concentration; details of the calculation of particle concentration of UCNPs are provided in the SI). As seen in Figure 2a–c, the luminescence quenching degree increases

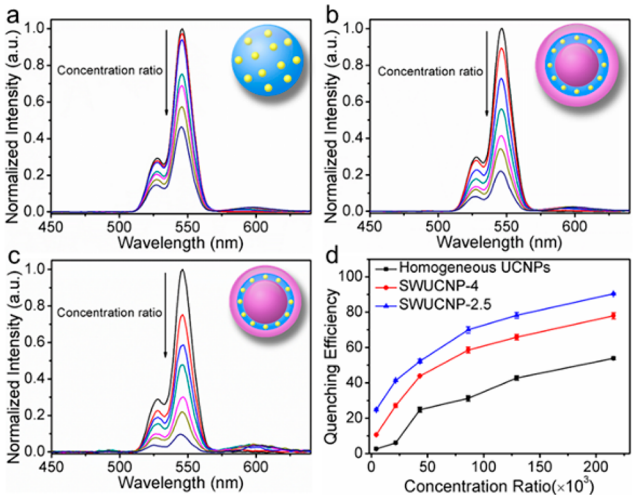

Figure 2. (a–c) Emission spectra of the three energy donors (with Er^{3+} as the emitting ions) at varying concentration ratios of dyes over UCNPs in MES buffer: (a) homogeneous UCNPs, (b) SWUCNP-4, and (c) SWUCNP-2.5. (d) Comparison on the quenching degrees of the three energy donors.

along with the concentration ratios of dyes over UCNPs for all three energy donors. Figure 2d clearly shows two outcomes of the comparison: (1) the luminescence quenching degrees of SWUCNPs are obviously enhanced as compared to homogeneous UCNPs; and (2) the quenching degree of SWUCNPs increases with reducing the thickness of the shells, i.e., from 4.0 to 2.5 nm, as a result of the distance-dependence of energy transfer. On the other hand, the emission of the energy acceptor can be another indicator of the LRET efficiency for a donor–acceptor pair. Our experiments show that the emission of the energy acceptor (dye) is rather weak when using homogeneous UCNPs as energy donor, while it becomes obvious with SWUCNPs as the donors. As illustrated in SI Figure S7, the ratio of emission intensity (dye-to-UCNPs) shows a moderate increase with SWUCNP-4 and a >7-fold enhancement with SWUCNP-2.5. The above results have unambiguously confirmed the validity of the sandwich structure for the enhancement of LRET efficiency. It is also revealed that the energy-transfer efficiency can be adjusted by tuning the thickness of the shell layers.

Fabrication of the SWUCNPs-Fluo-4 Nanoprobe. Commercially available Fluo-4 was selected as Ca^{2+} receptor for our probe, with BAPTA as the Ca^{2+} chelator[41,42] and fluorescein dye as the energy acceptor. Considering the absorption of fluorescein centering at 490 nm, we chose Tm^{3+} as the emitting ion for SWUCNPs to ensure the spectral match between energy donor and acceptor (SI Figure S8). Sandwich structured oleate-capped $NaYF_4$@$NaYF_4$:Yb,Tm@$NaYF_4$ nanoparticles were synthesized following the above procedure for SWUCNP-2.5, and the morphology was verified with TEM analysis (SI Figure S9a–c). In order to directly link Fluo-4 molecules to the surface of the SWUCNPs, so as to minimize the donor-to-acceptor distance, the oleate ligands were removed by acid treatment to obtain water-dispersible bared SWUCNPs (SI Figure S9d). Due to the removal of oleate ligands, Ln^{3+} ions are exposed on the surface of SWUCNPs, resulting in the weakening of the shoulder band at 2927 and 2852 cm^{-1} assigned to the asymmetric and symmetric stretching vibration of methylene ($-CH_2-$) in the long alkyl chain in FTIR spectra (Figure 3a) and a positive ζ potential of

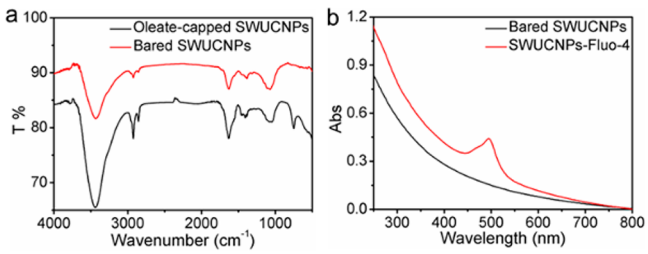

Figure 3. (a) FTIR spectra of the oleate-capped $NaYF_4$@$NaYF_4$:Yb,Tm@$NaYF_4$ SWUCNPs and bared $NaYF_4$@$NaYF_4$:Yb,Tm@$NaYF_4$ SWUCNPs. (b) The UV–vis absorption spectra of $NaYF_4$@$NaYF_4$:Yb,Tm@$NaYF_4$ SWUCNPs before and after attachment of Fluo-4.

+43.5 mV of the colloidal solution (SI Figure S10). The bared SWUCNPs are water-soluble and can be stably stored in water at room temperature for months at a high concentration (20 mg/mL). Because of the strong coordination capability of abundant lanthanide ions on the particle surface, the bared SWUCNPs can directly conjugate to biocompatible molecules with functional groups such as $-COOH$, $-NH_2$, and $-OH$ in water solution for further bio-application. The linkage of SWUCNPs and Fluo-4 was realized through the interaction between the carboxyl groups of BAPTA and the exposed lanthanide ions on surface of SWUCNPs (Scheme 1). The conjugation is confirmed by several approaches. After the attachment of Fluo-4, the ζ potential of particles shifts from +43.5 to +30.6 mV (SI Figure S10). Meanwhile, the absorption of fluorescein at 490 nm is clearly observed on the spectrum of SWUCNPs-Fluo-4 conjugate (Figure 3b). The obtained SWUCPs-Fluo-4 nanoprobe is well dispersed in aqueous solutions with long-period photostability.

***In Vitro* Ca^{2+} Assay in Aqueous Solution.** With the successful loading of Fluo-4, the luminescence of the SWUCNPs is quenched by fluorescein to a rate of 80% (SI

DOI: 10.1021/jacs.5b01504
J. Am. Chem. Soc. 2015, 137, 3421–3427

Figure S11). It is worth noting that the amount of Fluo-4 on the nanoprobe is as low as nmol level (~2.4 nmol/mg SWUCNPs). In this context, the 80% luminescence quenching represents a pretty high LRET efficiency, which further rationalizes our synergetic strategy combining confined emitters and bared surface of UCNPs. The LRET mechanism was also verified with time-resolved luminescence, which shows obvious reduction of the lifetime of SWUCNPs by Fluo-4 (SI Figure S12). As shown in Figure 4a, the photoluminescence of

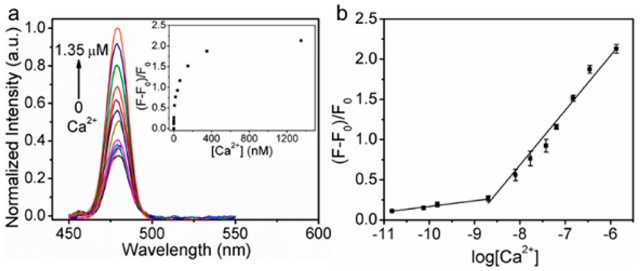

Figure 4. (a) Upconversion luminescence emission spectra of SWUCNPs-Fluo-4 (inset: luminescence titration curve), and (b) the relationship between the luminescence recovery and the logarithm of free Ca^{2+} concentration within the range from 15 pM to 1.35 μM (10 mM MOPS, 100 mM KCl, 10 mM EGTA, pH 7.2).

SWUCNPs is recovered in a $[Ca^{2+}]$-dependent manner. This nanoprobe is responsive to a free Ca^{2+} concentration lowered to picomolar level (Figure 4a inset). Figure 4b shows that the luminescence intensity recovery is linearly correlated to the logarithm of free Ca^{2+} concentration in the ranges from 15 pM to 1.5 nM and 1.5 nM to 1.35 μM, enabling quantitative detection of Ca^{2+} with an ultrahigh sensitivity and wide dynamic range. The two-stage linear response may be attributed to the competition between Ca^{2+} and UCNPs toward the carboxyl of Fluo-4,[43] which suggests that the Fluo-4 molecule can be detached from UCNPs surface only after it is completely chelated by Ca^{2+}. The photoluminescence of SWUCNPs-Fluo-4 before and after being subject to Ca^{2+} as a function of time was examined (SI Figure S13), which shows that the probe is quite stable without Ca^{2+} and affords a rapid response to Ca^{2+}. Notably, the quantification limit of 15 pM is significantly lower than most reported Ca^{2+} probes and indicators, e.g., it is at least 2 orders of magnitude lower than that obtained with Fluo-4. As a commercial calcium indicator, as we know, Fluo-4 itself also can quantify Ca^{2+} by employing the emission of fluorescein (excited with 490 nm) upon target binding (SI Figure S14, showing a quantification limit of 8 nM). And also, the dynamic range of SWUCNPs-Fluo-4 (15 pM to 1.35 μM) is far broader than that of Fluo-4 (8 nM to 0.064 μM, SI Figure S14). Since most cells in rest have a free Ca^{2+} concentration of 10−100 nM levels, this nanoprobe is sensitive enough for detection of cytosol $[Ca^{2+}]$. In addition, the SWUCNPs-Fluo-4 nanoprobe shows high specificity toward Ca^{2+} against other ions and biomolecules (SI Figure S15).

Tracking of Cytosol $[Ca^{2+}]$ in Living Cells. To evaluate the intracellular usage of the nanoprobe, the cytotoxicity of SWUCNPs-Fluo-4 was first investigated by the reduction activity of the methyl thiazolyl tetrazolium (MTT) assay. After incubation with SWUCNPs-Fluo-4 at concentrations ranging from 0 to 0.6 mg/mL for 24 h, the cell viability of HeLa cells was >90% (SI Figure S16), indicating a low cytotoxicity of the probe. We then used the nanoprobe to monitor intracellular Ca^{2+} level in living cells employing a microscope equipped with a 980 nm continuous laser. Altogether four groups of HeLa cells were investigated, which were treated with the probe, probe plus EGTA, probe with ATP, and probe with ATP and thapsigargin, respectively. We first assessed the uptake of the nanoprobe by cells. The single-cell Z-scanning by confocal microscopy confirms that the particles are successfully uptaken by cells and distribute in cytosol, indicating the fine biocompatibility of the as-constructed nanoprobe (Figure 5).

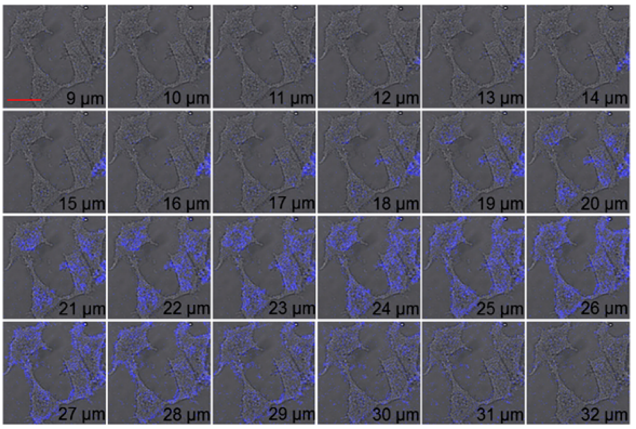

Figure 5. *Z*-direction slices of confocal luminescence imaging for HeLa cell after incubation with nanoprobe, ATP, and thapsigargin at 37 °C. Scale bar: 50 μm.

As shown in Figure 6b, HeLa cells incubated with the nanoprobe (0.3 mg/mL) for 1.5 h exhibit weak luminescence, which can be assigned to the existence of low concentration Ca^{2+} in resting cells. In a negative control group, the cells were pretreated with ethylene glycol tetraacetic acid (EGTA), a membrane-permeable Ca^{2+} chelator that can effectively remove Ca^{2+},[44] followed by incubation with the nanoprobe for 1.5 h. As seen in Figure 6a, even weaker luminescence of UCNPs is observed because of the depletion of cytosol Ca^{2+} by EGTA. Further, two positive control groups were tested to observe $[Ca^{2+}]$ elevation. One group of cells was treated with adenosine triphosphate (ATP, 20 μM), which can stimulate cells to release free Ca^{2+} from endoplasmic reticula to cytosol, after incubation with the nanoprobe. In this case, the luminescence of the nanoprobe is obviously enhanced (Figure 6c). The other group was treated with both ATP (20 μM) and thapsigargin (5 μM), an agent inhibiting the influx of Ca^{2+} from cytosol into the endoplasmic reticula (ER).[45] The enhancement of upconversion luminescence is more obvious in this group (Figure 6d). Moreover, owing to the high sensitivity and stability of the nanoprobe, the dynamic change of intracellular $[Ca^{2+}]$ upon ATP stimulation is detectable, which reveals the rapid rise in $[Ca^{2+}]$ of living cells in response to external ATP (Figure 6f). The kinetic signal in Figure 6f (as well as that in Figure S13) also suggests an irreversible response mechanism of the nanoprobe toward Ca^{2+}. To preclude the possible contribution of EGTA or ATP to the increase of upconversion emission, two sets of control experiments were conducted, where the probe was incubated with EGTA or ATP in the absence of calcium. It is seen that, in the absence of calcium, the luminescence of the probe keeps almost unchanged (SI Figure S17). Taken together, these results have confirmed the capability of the SWUCNPs-based nanoprobe in tracking of cytosol $[Ca^{2+}]$.

DOI: 10.1021/jacs.5b01504
J. Am. Chem. Soc. 2015, 137, 3421−3427

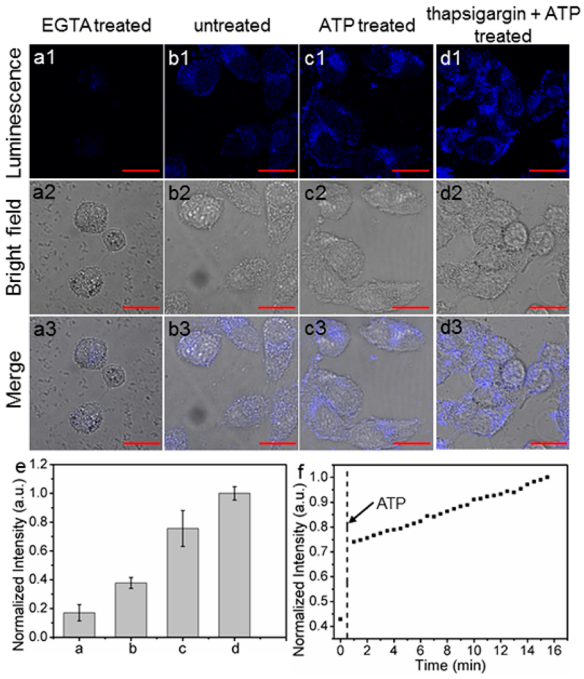

Figure 6. (a–d) Upconversion luminescence imaging of Hela cells. (a) Cells treated with EGTA (50 μM) for 10 min followed by incubation with SWUCNPs-Fluo-4; (b) SWUCNPs-Fluo-4-labeled HeLa cells; (c) cells incubated with SWUCNPs-Fluo-4 for 1.5 h followed by treating with ATP (20 μM); (d) cells pretreated with thapsigargin (5 μM) for 10 min followed by incubation with SWUCNPs-Fluo-4 and ATP (20 μM). (e) Normalized mean luminescence intensities of images (a–d). (f) Time course of upconversion luminescence of HeLa cells after stimulation with ATP. Images were collected at 450–500 nm with 30 s intervals. Scale bar: 50 μm.

Ca^{2+} Imaging in Mice Liver Tissues. We further checked whether the nanoprobe can be delivered to organs and light up the target *in vivo*. As previously reported, the calcitonin produced by C-cells can facilitate the entry of extracellular calcium into liver cells by opening Ca^{2+} channels located on the plasma membranes. As a consequence, liver Ca^{2+} content can be significantly increased after an i.p. injection of external Ca^{2+}.[46] Thus, we applied the SWUCNPs-Fluo-4 nanoprobe to detect the alteration of liver Ca^{2+} content using a mouse model. As can be seen from Figure 7, the nanoprobes are uniformly distributed in the tissue, which again verifies the compatibility of the nanoprobe in the biological samples. Figure 7b–d shows that the liver Ca^{2+} content is elevated stepwise with increasing the amount of injected $CaCl_2$. In a negative control group, the mice were pretreated with EGTA (10 mg/100 g body weight) which can chelate Ca^{2+} and induce hypocalcaemia,[47] followed by injection of the nanoprobe. As seen in Figure 7a, the luminescence of UCNPs is considerably weakened because of the depletion of liver Ca^{2+}. This result is consistent with the above observation obtained with cultured cells. A more complicated group was designed to test the inhibition of extracellular calcium influx into liver cells. This group of mice was pretreated with verapamil (1.0 mg/100 g body weight in 200 μL physiological saline), a Ca^{2+} channel blocker,[46] before the injection of $CaCl_2$. In this case, the luminescence intensity is weaker than that of the group injected with the same dosage of $CaCl_2$ (Figure 7e) and is close to the resting cells (Figure 7b). These observations demonstrate that the SWUCNPs-Fluo-4 nanoprobe can be applied to monitor Ca^{2+} content in mouse liver tissue.

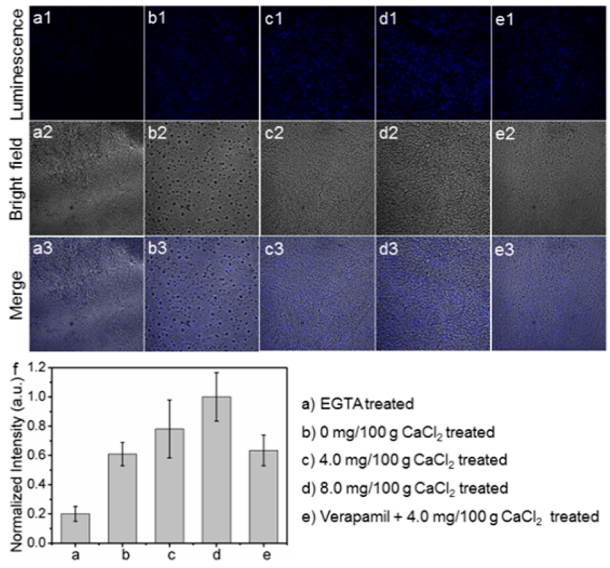

Figure 7. (a–e) Upconversion luminescence imaging of mouse liver slice. (a) Mice injected with EGTA (10 mg/100 g (body weight, same as below)) for 30 min before the injection of SWUCNPs-Fluo-4 nanoprobes; (b–d) mice injected with $CaCl_2$ (b: 0 mg/100 g, c: 4.0 mg/100 g, d: 8.0 mg/100 g) for 30 min followed by injection with SWUCNPs-Fluo-4 nanoprobe; (e) mice pretreated with verapamil (1.0 mg/100 g) for 30 min before the injection of $CaCl_2$. (f) Normalized luminescence intensities of images (a–e).

CONCLUSION

In summary, we have proposed a new LRET-based NIR nanoprobe for calcium, using UCNPs with confined emitters and bared surface as the energy donor. Our synergetic strategy affords significantly improved LRET efficiency and ultrahigh sensitivity. The layer-by-layer seed-mediated shell growth method is able to precisely control the morphology and specifically localize the emitting ions in the inner shell of the material, which offers the opportunity to further refine the LRET efficiency by tuning the thickness of the shell layers. The probe fabricated by directly linking target receptors on bared surface of the nanoparticles is stable and noncytotoxic, ensuring the biocompatibility and long-term observation in living cells. The LRET-based upconversion nanoprobe is able to trace cytosol [Ca^{2+}] in cultured cells and detect Ca^{2+} content in mice liver tissues. Our strategy can be generalized to construct various upconversion nanoprobes by simply changing the Ca^{2+} receptor into other recognition units, such as peptides, aptamers and small-molecule ligands.

ASSOCIATED CONTENT

Supporting Information

Experimental details, the XRD, TEM, FTIR characterization of SWUCNPs, the results of ζ potential measurements, the cell viability of nanoprobe, and control experiments. This material is available free of charge via the Internet at http://pubs.acs.org.

AUTHOR INFORMATION

Corresponding Author

*zhhliu@whu.edu.cn

DOI: 10.1021/jacs.5b01504
J. Am. Chem. Soc. 2015, 137, 3421–3427

Notes

The authors declare no competing financial interest.

■ ACKNOWLEDGMENTS

This work has been financially supported by the National Natural Science Foundation of China (no. 21375098) and the National Basic Research of China (973 program, no. 2011CB933600). The authors are grateful to Prof. Xueyuan Chen and Dr. Datao Tu for their help with lifetime measurements.

■ REFERENCES

(1) Wang, G. F.; Peng, Q.; Li, Y. D. *Acc. Chem. Res.* **2011**, *44*, 322.
(2) Achatz, D. E.; Ali, R.; Wolfbeis, O. S. *Top. Curr. Chem.* **2011**, *300*, 29.
(3) Zhou, J.; Liu, Z.; Li, F. Y. *Chem. Soc. Rev.* **2012**, *41*, 1323.
(4) Soukka, T.; Rantanen, T.; Kuningas, K. *Ann. N.Y. Acad. Sci.* **2008**, *1130*, 188.
(5) Wang, F.; Liu, X. G. *Chem. Soc. Rev.* **2009**, *38*, 976.
(6) Sun, L. D.; Wang, Y. F.; Yan, C. H. *Acc. Chem. Res.* **2014**, *47*, 1001.
(7) Liu, Y. S.; Tu, D. T.; Zhu, H. M.; Chen, X. Y. *Chem. Soc. Rev.* **2013**, *42*, 6924.
(8) Haase, M.; Schäfer, H. *Angew. Chem., Int. Ed.* **2011**, *50*, 5808.
(9) Wang, F.; Han, Y.; Lim, C. S.; Lu, Y. H.; Wang, J.; Xu, J.; Chen, H. Y.; Zhang, C.; Hong, M. H.; Liu, X. G. *Nature* **2010**, *463*, 1061.
(10) Dai, Y. L.; Xiao, H. H.; Liu, J. H.; Yuan, Q. H.; Ma, P. A.; Yang, D. M.; Li, C. X.; Cheng, Z. Y.; Hou, Z. Y.; Yang, P. P.; Lin, J. *J. Am. Chem. Soc.* **2013**, *135*, 18920.
(11) Xiao, Q. F.; Zheng, X. P.; Bu, W. B.; Ge, W. Q.; Zhang, S. J.; Chen, F.; Xing, H. Y.; Ren, Q. G.; Fan, W. P.; Zhao, K. L.; Hua, Y. Q.; Shi, J. L. *J. Am. Chem. Soc.* **2013**, *135*, 13041.
(12) Li, L. L.; Zhang, R. B.; Yin, L. L.; Zheng, K. Z.; Qin, W. P.; Selvin, P. R.; Lu, Y. *Angew. Chem., Int. Ed.* **2012**, *51*, 6121.
(13) Achatz, D. E.; Merier, R. J.; Fischer, L. H.; Wolfbeis, O. S. *Angew. Chem., Int. Ed.* **2011**, *50*, 260.
(14) Wang, L. Y.; Yan, R. X.; Huo, Z. Y.; Wang, L.; Zeng, J. H.; Bao, J.; Wang, X.; Peng, Q.; Li, Y. D. *Angew. Chem., Int. Ed.* **2005**, *44*, 6054.
(15) Liu, J. N.; Liu, Y.; Bu, W. B.; Bu, J. W.; Sun, Y.; Du, J. L.; Shi, J. L. *J. Am. Chem. Soc.* **2014**, *136*, 9701.
(16) Li, Z. Q.; Zhang, Y.; Jiang, S. *Adv. Mater.* **2008**, *20*, 4765.
(17) Wang, M.; Hou, W.; Mi, C. C.; Wang, W. X.; Xu, Z. R.; Teng, H. H.; Mao, C. B.; Xu, S. K. *Anal. Chem.* **2009**, *81*, 8783.
(18) Meier, R. J.; Simbürger, J. M. B.; Soukka, T.; Schäferling, M. *Anal. Chem.* **2014**, *86*, 5535.
(19) Liu, Y.; Chen, Min.; Cao, T. Y.; Sun, Y.; Li, C. Y.; Liu, Qian.; Yang, T. S.; Yao, L. M.; Feng, W.; Li, F. Y. *J. Am. Chem. Soc.* **2013**, *135*, 9869.
(20) Chen, G. Y.; Qiu, H. L.; Prasad, P. N.; Chen, X. Y. *Chem. Rev.* **2014**, *114*, 5161.
(21) Zhang, P.; Rogelj, S.; Nguyen, K.; Wheeler, D. *J. Am. Chem. Soc.* **2006**, *128*, 12410.
(22) Kuningas, K.; Ukonaho, T.; Päkkilä, H.; Rantanen, T.; Rosenberg, J.; Lövgren, T.; Soukka, T. *Anal. Chem.* **2006**, *78*, 4690.
(23) Yuan, Y. X.; Liu, Z. H. *Chem. Commun.* **2012**, *48*, 7510.
(24) Rantanen, T.; Järvenpää, M. L.; Vuojola, J.; Kuningas, K.; Soukka, T. *Angew. Chem., Int. Ed.* **2008**, *47*, 3811.
(25) Wang, C.; Banerjee, D.; Liu, Y. S.; Chen, X. Y.; Liu, X. G. *Analyst* **2010**, *135*, 1839.
(26) Lakowicz, J. R. *Principles of Fluorescence Spectroscopy*, 2nd ed.; Kluwer Academic: New York, 1999.
(27) Chen, Z. G.; Chen, H. L.; Hu, H.; Yu, M. X.; Li, F. Y.; Zhang, Q.; Zhou, Z. G.; Yi, T.; Huang, C. H. *J. Am. Chem. Soc.* **2008**, *130*, 3023.
(28) Zheng, W.; Zhou, S. Y.; Chen, Z.; Hu, P.; Liu, Y. S.; Tu, D. T.; Zhu, H. M.; Li, R. F.; Huang, M. D.; Chen, X. Y. *Angew. Chem., Int. Ed.* **2013**, *52*, 6671.
(29) Wang, F.; Wang, J.; Liu, X. G. *Angew. Chem., Int. Ed.* **2010**, *49*, 7456.
(30) Zhang, C. L.; Yuan, Y. X.; Zhang, S. M.; Wang, Y. H.; Liu, Z. H. *Angew. Chem., Int. Ed.* **2011**, *50*, 6851.
(31) Wu, S. J.; Duan, N.; Ma, X. Y.; Xia, Y.; Wang, H. X.; Wang, Z. P.; Zhang, Q. *Anal. Chem.* **2012**, *84*, 6263.
(32) Wang, Y. H.; Wu, Z. J.; Liu, Z. H. *Anal. Chem.* **2013**, *85*, 258.
(33) Wei, Y.; Lu, F. Q.; Zhang, X. R.; Chen, D. P. *Chem. Mater.* **2006**, *18*, 5733.
(34) Liu, C. H.; Wang, H.; Li, X.; Chen, D. P. *J. Mater. Chem.* **2009**, *19*, 3546.
(35) Liu, C. H.; Wang, H.; Zhang, X. R.; Chen, D. P. *J. Mater. Chem.* **2009**, *19*, 489.
(36) Li, L. L.; Wu, P. W.; Hwang, K.; Lu, Y. *J. Am. Chem. Soc.* **2013**, *135*, 2411.
(37) Bogdan, N.; Vetrone, F.; Ozin, G. A.; Capobianco, J. A. *Nano Lett.* **2011**, *11*, 835.
(38) Huang, P.; Zheng, W.; Zhou, S. Y.; Tu, D. T.; Chen, Z.; Zhu, H. M.; Li, R. F.; Ma, E.; Huang, M. D.; Chen, X. Y. *Angew. Chem., Int. Ed.* **2014**, *53*, 1252.
(39) Tsien, R. Y.; Pozzan, T.; Rink, T. J. *J. Cell Biol.* **1982**, *94*, 325.
(40) Bagh, S.; Paige, M. F. *J. Phys. Chem. A* **2006**, *110*, 7057.
(41) Tsien, R. Y. *Biochemistry* **1980**, *19*, 2396.
(42) Tsien, R. Y. *Nature* **1981**, *290*, 527.
(43) Li, T.; Wang, E. K.; Dong, S. J. *Anal. Chem.* **2010**, *82*, 1515.
(44) Mohan, P. S.; Lim, C. S.; Tian, Y. S.; Roh, W. Y.; Lee, J. H.; Cho, B. R. *Chem. Commun.* **2009**, *36*, 5365.
(45) Inesi, G.; Hua, C.; Xu, C.; Ma, H.; Seth, M.; Prasad, A. M.; Sumbilla, C. *J. Bioenerg. Biomembr.* **2005**, *37*, 365.
(46) Yamaguchi, M.; Yoshida, H. *Acta Endocrinol.* **1985**, *110*, 239.
(47) Wang, W.; Lewin, E.; Olgaard, K. *Eur. J. Clin. Invest.* **2002**, *32*, 674.

DOI: 10.1021/jacs.5b01504
J. Am. Chem. Soc. 2015, 137, 3421−3427